RSC Advances

PAPER

View Article Online
View Journal | View Issue

Cite this: *RSC Adv.*, 2015, **5**, 10816

Effect of functional groups on dielectric, optical gas sensing properties of graphene oxide and reduced graphene oxide at room temperature†

T. Kavinkumar,[a] D. Sastikumar[b] and S. Manivannan*[a]

Graphene oxide (GO) was synthesized from graphite through a chemical oxidation process and heat treated at 110 and 220 °C in a vacuum atmosphere. The partial reduction and sp^3 to sp^2 phase transition of GO was characterized by powder X-ray diffraction, Fourier-transform infrared, micro Raman, ultraviolet-visible-near infrared spectroscopy techniques. Dielectric properties of pristine GO and heat-treated GO were studied in the frequency range 10^2 to 10^6 Hz at 27 °C. Hydroxyl, carboxyl functional groups removed GO after 220 °C heat treatment, expressed higher electrical conductivity, dielectric constant and dielectric loss in the order of 10^{-2} S m^{-1}, 10^3 and 10^5 respectively than the pristine GO (10^{-6} S m^{-1}, 10^1 and 10^1). Pristine and heat-treated GO were coated on the partially cladding removed poly-methyl methacrylate optical fiber and used as fiber optic gas sensors. GO and heat treated GO coated fibers were responsive to detect ammonia, ethanol and methanol vapors from 0 to 500 ppm at 27 °C. Sensitivities of GO coated fiber optic sensor were calculated as −0.32, −0.26 and −0.20 counts per ppm for ammonia, ethanol and methanol vapors respectively. The effect of functional groups on dielectric and gas sensing properties of GO was investigated and reported.

Received 20th October 2014
Accepted 6th January 2015

DOI: 10.1039/c4ra12766h

www.rsc.org/advances

Introduction

Graphene is a fundamental building block of carbon materials as it consists of two-dimensional sp^2-bonded carbon sheets. It plays an important role in science, engineering and technology because of its excellent mechanical, thermal and electrical properties.[1–3] In the past few years, high quality graphene sheets have been obtained by several methods including scotch tape,[4] chemical/thermal reduction,[5] chemical vapor deposition (CVD)[6] and epitaxial growth.[7] Among them, economic bulk production of graphene has been realized through the reduction of graphene oxide (GO). Covalently decorated functional groups such as hydroxyl, epoxides present on the basal planes, carbonyl and carboxyl groups at the edges of graphene layers result in thermally unstable GO nanomaterial. GO consisting of thick two-dimensional sheets became electrically nonconductive and strongly hydrophilic due to the presence of more sp^3 and less sp^2 carbon atoms. The excellent physical and mechanical properties of GO finds potential application in nanoelectronics, polymer composite, bio-medicine, sensor and photovoltaic devices.[8–12] Removal of oxygen functional groups from the surface of GO have been realized through chemical and thermal methods.[13] Most commonly used reducing agents are hydrazine,[5] sodium borohydride,[14] hydroquinone[15] and ascorbic acid.[16] Compared to the chemical method, thermal treatment is environmentally friendly and offers high quality graphene. The rGO and graphene have the tendency to settle down quickly after the dispersion in ethanol, water and ethylene glycol. This is due to the removal of functional groups from GO after the reduction. The functional groups in GO will help us to tune the electrical and gas sensing properties.

Recently, GO and graphene are widely used as active materials to detect the gas molecules. Oxygenated sheets of graphene sensor has very high surface area and develop the better gas detection abilities than its counterpart due to adsorption of gas molecules on the surface of sheets.[17,18] Some *et al.* demonstrated the gas sensors using hydrophilic GO and hydrophobic reduced graphene oxide (rGO) to sense the volatile organic gases. It is reported that the sensitivity of GO is higher than the rGO. This is due to high surface area and presence of different functional groups in GO.[19] On the other hand, Huang *et al.* reported *in situ* investigation on the transition of electrical properties of GO paper from −40 to 150 °C. *In situ* dielectric spectroscopy studies revealed the four stage transition of electrical properties of GO with increasing temperature.[20] The above reports clearly indicates the potential of GO and rGO towards the gas sensing and flexible electronic device applications.

[a]*Carbon Nanomaterials Laboratory, Department of Physics, National Institute of Technology, Tiruchirappalli 620 015, India. E-mail: ksmani@nitt.edu; ksmaniphysics@yahoo.com; Fax: +91-431-2500133; Tel: +91-431-2503616*

[b]*Department of Physics, National Institute of Technology, Tiruchirappalli 620 015, India*

† Electronic supplementary information (ESI) available. See DOI: 10.1039/c4ra12766h

But, for practical applications, room temperature operation of gas sensor and flexible electronic devices require well defined characteristics of GO and rGO. Hence, it is important to understand the role of functional groups towards the gas sensing and dielectric properties. The present work focus on tailor made synthesis of GO through heat treatment processes. For the first time, the role of hydroxyl, carboxyl functional groups on dielectric and optical gas sensing properties of GO, heat treated GO for ammonia, ethanol and methanol vapors is reported.

Experimental section

Preparation of GO free standing films

GO was prepared from commercial graphite powder (Alfa Aesar 250 mesh) using the modified Hummers method reported elsewhere.[21] Stable dispersion of the synthesized GO was achieved by direct exfoliation in double distilled water under sonication for 60 min at 30 °C. Free standing GO paper was prepared by vacuum filtration method from the colloidal solution of GO using Teflon coated, 300 nm membrane filter. Thickness of the GO paper was measured as 50 μm using field emission scanning electron microscope (FESEM). The GO paper was annealed at 110, 220 °C in a vacuum furnace for 30 min and used for further studies. The *in situ* thermal reduction of GO is schematically presented in Fig. 1. The surface and edges of GO were attached with different oxygen functional groups such as carboxyl, hydroxyl and epoxides. The presence of functional groups increase the interlayer spacing of GO and was calculated as 0.930 nm. Reduced interlayer spacing was obtained after the thermal treatment of GO. This was due to the loss of functional groups which increased the van der Waals interaction between the GO layers.

Characterization

Powder X-ray diffraction (XRD) pattern was recorded (Rigaku Ultima III) at a scanning rate of 0.2° min^{-1} in the range of 5–80° with CuKα_1 radiation (1.5406 Å). Fourier-transform infrared (FT-IR) spectra of all samples were collected using Thermo-Scientific Nicolet IS5 spectrophotometer in the range 4000–1000 cm^{-1}. Thermogravimetric analyses (TGA) was carried out in the temperature range 30–800 °C at the heating rate of 20 °C min^{-1} under N_2 atmosphere (SIINT, EXSTAR 6200). Ultraviolet-visible-near infrared (UV-vis-NIR) studies were carried out in the range of 200–800 nm using JASCO UV-vis-NIR (Model-V-670) spectrophotometer. The microstructure of sample was obtained using Princeton Acton SP2500 Raman spectrometer with an excitation wavelength of 514.5 nm laser beam. The morphology of GO nanosheets and thickness were estimated using a FESEM (Quanta 250 FEG, FEI). Room temperature dielectric measurement was carried out in the frequency range 10^2 to 10^6 Hz (HIOKI 3532-50). The 1 cm^2 GO free standing film was sandwiched between two silver electrodes to make ohmic contacts on both sides of the paper. Dielectric study of the material develops the understanding about the electrical properties with respect to applied frequency, where the complex permittivity is given by[22]

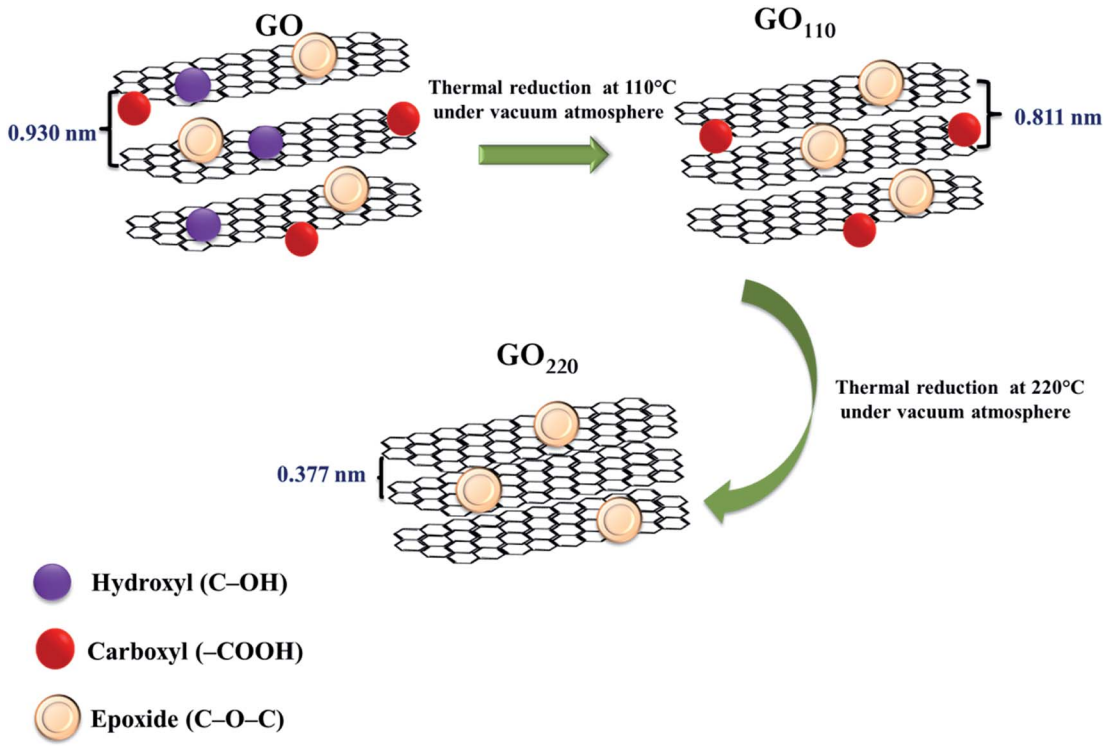

Fig. 1 Schematic diagram for the decomposition of oxygen functional groups from GO sheets.

$$\varepsilon^*(\omega) = \varepsilon'(\omega) - i\varepsilon''(\omega) \quad (1)$$

where ε' and ε'' are the real and imaginary parts of complex dielectric constant respectively. $\omega = 2\pi f$ is the angular frequency and f is the applied frequency. Dielectric loss of a material is known from the dissipation factor or loss tangent, which is given by

$$\tan\delta(\omega) = \frac{\varepsilon''(\omega)}{\varepsilon'(\omega)} \quad (2)$$

The real part of dielectric constant is derived from the following relation,

$$\varepsilon'(\omega) = \frac{Cd}{\varepsilon_0 A} \quad (3)$$

where C, is the measured capacitance in Farad, d and A correspond to thickness and cross sectional area of the GO paper in meter and m^2 respectively, ε_0 is the permittivity of free space, $= 8.85 \times 10^{-12}$ F m^{-1}. The complex electric modulus was calculated from the complex permittivity. The real (M') and imaginary (M'') parts of the electric modulus are derived using the real and imaginary parts of the dielectric constant as follows

$$M' = \frac{\varepsilon'}{\varepsilon'^2 + \varepsilon''^2} \quad (4)$$

$$M'' = \frac{\varepsilon''}{\varepsilon'^2 + \varepsilon''^2} \quad (5)$$

The AC conductivity (σ) was calculated by the following equation[20]

$$\sigma = \varepsilon_0 \varepsilon' \omega \tan\delta \quad (6)$$

Preparation of fiber optic gas sensor

Gas sensing properties were studied using homemade fiber-optic experimental setup with white light source (100–2000 nm, Model: SL1, Steller Net Inc., USA) and a miniature fiber optic spectrometer (100–1100 nm, Model: EPP-2000, Stellar Net Inc., USA). Signal in the form of light observed using the spectrometer was interfaced with a computer and the spectral response of the fiber was recorded independently for ammonia, ethanol and methanol vapors as reported earlier.[23,24]

The multimode step index poly-methyl methacrylate (PMMA) fiber cladding region was removed over 3 cm long at the center of 42 cm long fiber adapting mechanical cleaving method. The cladding removed fiber was then polished and its uniformity was observed through an optical microscope after cleaning with ethanol. Diameter of PMMA fiber was 750 μm (core = 735 μm, cladding = 15 μm, NA = 0.51) with the refractive index of 1.492 and 1.402 for core and cladding respectively. The as prepared GO and heat-treated GO_{110}, GO_{220} were coated independently over the cladding removed areas of fibers using the dip coating method and then dried in air. The prepared fiber optic gas sensor was inserted into the gas sensing chamber. The schematic diagram of experimental set up for the gas sensing measurement is depicted in Fig. 2. Ammonia, ethanol and methanol vapors prepared at different concentrations (0–500 ppm) were allowed separately to pass into the gas sensing chamber through a gas inlet with the help of a regulator. After 10 min of passing the vapor, variation of output light intensity was continuously measured for each concentration. All the measurements were made at 27 °C.

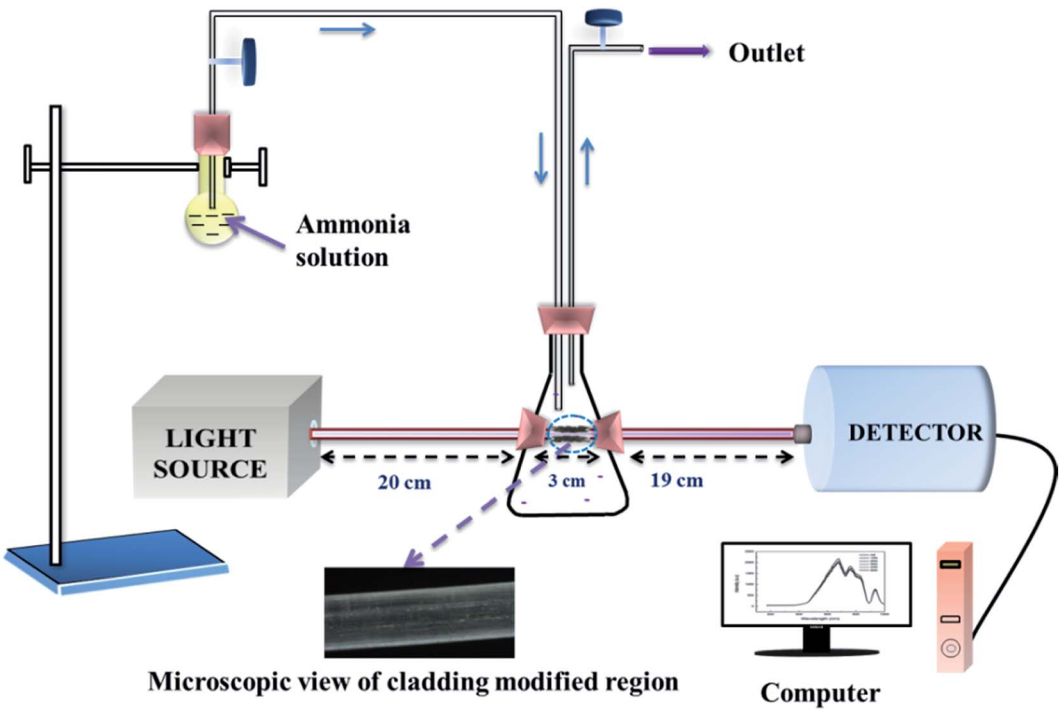

Fig. 2 Schematic diagram of fiber optic gas sensor setup.

Results and discussion

Fig. 3 shows the powder XRD patterns of graphite, GO, GO_{110} and GO_{220}. The GO and graphite showed the maximum intensity at 9.5° and 26.3° respectively corresponding to interlayer spacing of 0.930 nm and 0.338 nm. The maximum intensity at $2\theta = 9.5°$ confirms the graphite was totally oxidized into GO. The intercalation of water molecules, various oxygen functional groups attached on the basal planes, edges and the sp^3 bonding defects generated on the uniform graphene sheets were responsible for greater interlayer spacing of GO than the graphite. When GO was heated at 110 °C, the maximum intensity was slightly shifted to $2\theta = 10.9°$, corresponding interlayer spacing of 0.811 nm indicating the removal of physically adsorbed water molecules and oxygen functional groups. Characteristic diffracted pattern of GO was disappeared and broad pattern appeared at 23.6° corresponding to interlayer spacing of 0.377 nm when the sample was heated at 220 °C. This broad and weak pattern suggested that the presence of graphene sheets in the GO_{220}. This confirms the majority of oxygen functional groups were removed from the graphene sheets.[25]

FT-IR spectra of graphite, GO, GO_{110} and GO_{220} were presented in Fig. 4 and the assignment was given in Table 1. No absorption peak from graphite confirmed the absence of functional groups in the commercial graphite powder. The absorption peaks at 1725, 3416, 1054 and 1383 cm^{-1} in GO evidenced the presence of C=O, O–H, C–O and C–OH functional groups respectively. The removal of functional groups from GO after the heat treatments at 110 and 220 °C was responsible for the reduced peak intensity. Nevertheless, the presence of weak absorption peaks, established the GO was partially reduced after the heat treatment processes. The water molecules were evaporated from GO at 110 °C and hence the reduction in O–H peak intensity of GO_{110}. The vibrations of remaining functional groups attached with GO_{110} are matching with the functional groups in GO. This result supported that the heat treatment did not disturbed the core structure of GO. Meanwhile, most of the functional groups were disappeared from GO after the 220 °C heating. However, the trace of functional groups in the honeycomb carbon structure introduced the limitations of the chemical reduction of GO.[26]

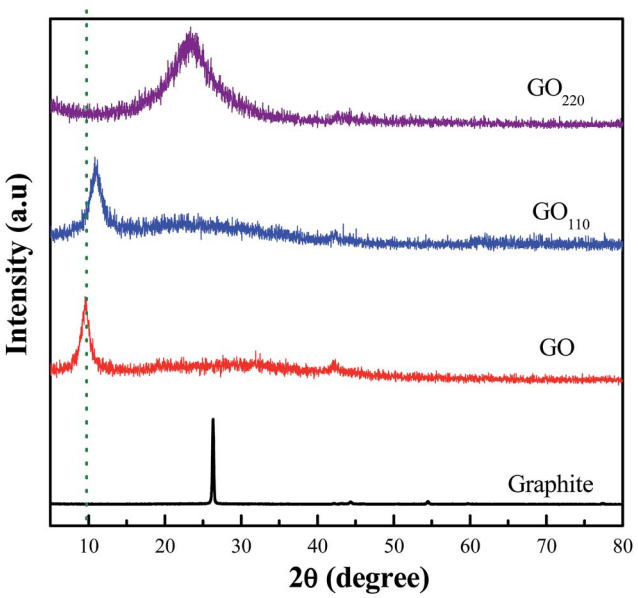

Fig. 3 XRD patterns of graphite, pristine GO, GO_{110} and GO_{220}.

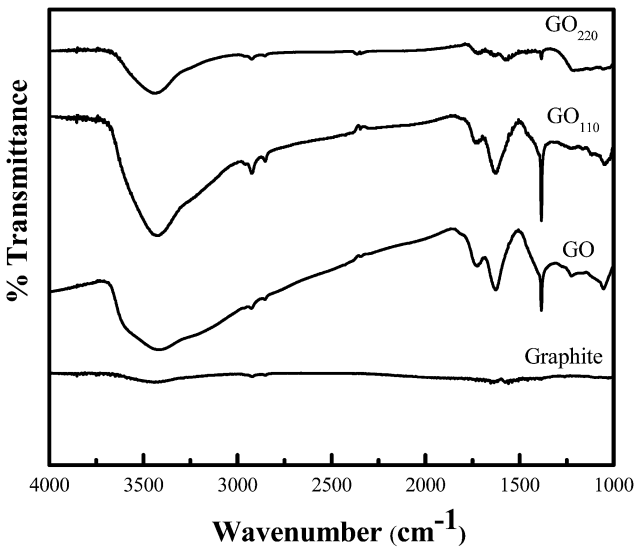

Fig. 4 FT-IR spectra of graphite, pristine GO, GO_{110} and GO_{220}.

The thermal stability of graphite and GO was calculated using TGA (Fig. 5). Graphite showed better thermal stability than GO. Linear relationship was noticed between weight loss and temperature for graphite. Meantime, there were three major steps of weight losses observed for GO. The weight loss was about 20% at around 110 °C, attributed to the removal of loosely bounded, adsorbed water and gas molecules. About 50% of weight loss occurred at around 220 °C, was ascribed to the elimination of O_2, CO and CO_2. This confirmed that highly reactive oxygen atoms from the GO structure react well to form CO and CO_2. Further, weight loss at about 500 °C indicates the further reduction process of GO. Substantial weight loss was observed when GO was heated beyond 500 °C indicating the absence of major oxygen functional groups.

Raman spectroscopy (Fig. 6) evidenced the occurrence of structural changes due to the chemical treatment, from graphite to GO and the thermal treatment of GO to the partially reduced GO. Raman spectrum of graphite showed the low intense D band at 1361 cm^{-1} and was used to measure the defects, arising from a breathing mode of *k*-point phonons of A_{1g} symmetry. The intense G band corresponds to the first-order scattering of E_{2g} mode of sp^2 carbon and was observed at 1575 cm^{-1}. Presence of functional groups such as hydroxyl, epoxy generated the disorder in GO. Raman spectrum of as prepared GO showed relatively high D band at 1344 cm^{-1} and the G band was shifted to 1596 cm^{-1} compared to graphite. Transformation of sp^3 to sp^2 and degree of disorder were indicated by the intensity ratio of D band and G band (I_D/I_G). The I_D/I_G was inversely proportional to the average size of the sp^2 domains.

Table 1 The assignment of functional groups in FTIR spectra

		Origin and nature			
Peak position (cm^{-1})	Assignment	Graphite	GO	GO_{110}	GO_{220}
1054	C–O stretching	No absorption peak	Strong	Strong	Weak
1383	C–OH stretching	No absorption peak	Strong	Strong	Weak
1623	C=C stretching	Weak	Strong	Strong	Weak
1725	C=O stretching	No absorption peak	Strong	Strong	Weak
3416	O–H stretching	Weak	Broad	Weak peak compared to GO	Very weak

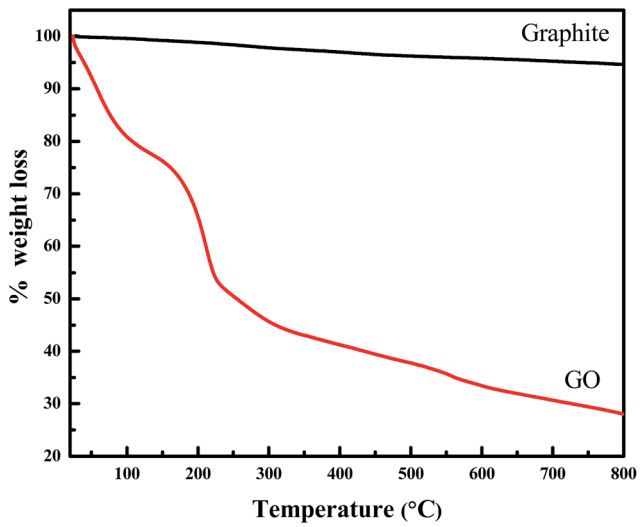

Fig. 5 TGA of graphite and GO.

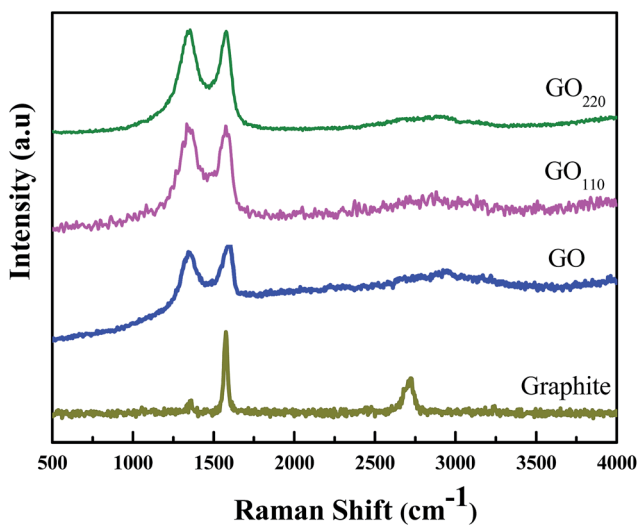

Fig. 6 Raman spectra of graphite, pristine GO, GO_{110} and GO_{220}.

Variations of I_D/I_G will lead to the changes in the electronic conjugation state of the GO during the thermal reduction. The Raman spectrum of GO_{110} displayed the prominent D and G bands at 1350 and 1578 cm^{-1} respectively. Meanwhile, the increased intensity ratio as 0.98 for GO_{110} compared to GO (0.94) was due to elimination of water molecules from the graphene sheets. The I_D/I_G ratio increased further to 1.01 when the sample was annealed at 220 °C and was higher than GO and GO_{110}. This confirmed the effective removal of defects/restoration of sp^2 carbon atoms and reduced sizes of the sp^2 domains.

Fig. 7a shows the FESEM image of cross-sectional view of vacuum dried free standing GO paper obtained by filtration of GO dispersion in water. Fig. 7b witnessed that the oxygenated graphene sheets were highly exfoliated having layered structure. This qualitative information reinforced the XRD observation on the expansion of interlayer spacing from 0.338 nm (graphite) to 0.930 nm.

UV-vis-NIR spectra of GO and heat-treated GO are shown in Fig. 8. GO exhibits the maximum absorbance at 230 nm originated from the π–π* transition of C–C and C=C in sp^2 hybrid regions, whereas a small hump at 300 nm was due to n–π* transition of the C=O in sp^3 hybrid regions. However, the absorption peak of π–π* transition was shifted to the higher wavelength 238 nm for GO_{110} and the shoulder peak at 300 nm

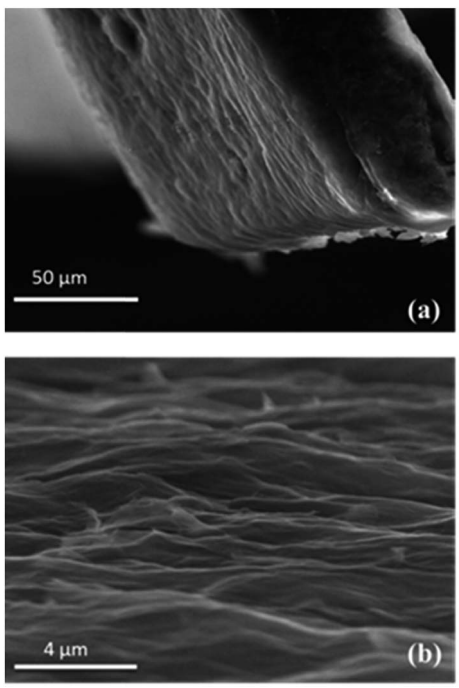

Fig. 7 FE-SEM image of (a) side-view of thick pristine GO paper, (b) layered and exfoliated GO sheets.

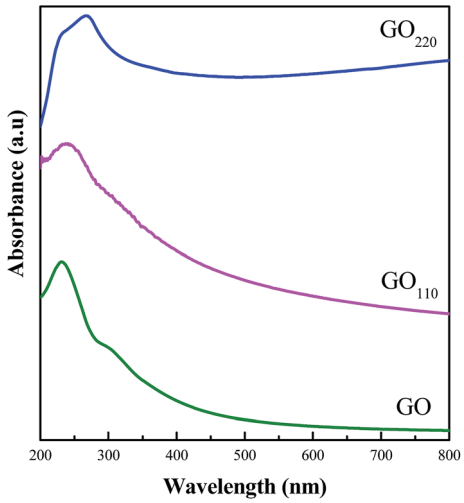

Fig. 8 UV-vis-NIR absorption spectra of pristine GO, GO_{110} and GO_{220} dispersed in ethylene glycol.

was also started to disappear, indicating the water containing functional groups on the GO surface were removed partially. The absorption peak of GO_{220} for π–π^* transition of C–C was shifted to 273 nm. This was due to the removal of some oxygen functional groups and restoration of C=C bonds in GO_{220} sheets. This result supports the FT-IR observation on the presence and absence of oxygen functional groups in GO and GO_{220} nanosheets respectively.

Fig. 9 shows the frequency dependence of AC electrical conductivity calculated for GO, GO_{110} and GO_{220} papers at 27 °C. The GO paper was considered as layered composite consists of insulating sp^3 matrix and conductive sp^2 clusters.[20] The pristine GO paper exhibits frequency dependent electrical conductivity and it increases with increasing frequency. The conductivity showed less variation when the applied frequency was low due to more active grain boundaries. Variation at high

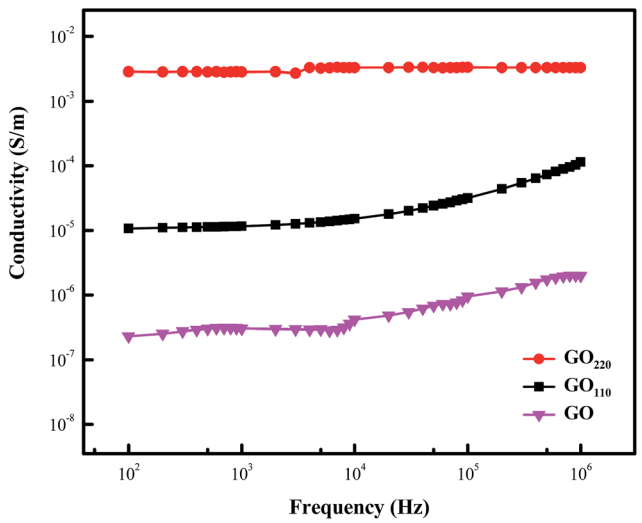

Fig. 9 The variation of electrical conductivity against the applied frequency of pristine GO, GO_{110} and GO_{220}.

frequency regions was due to less active grain boundaries. Intercalated water molecules and additional oxygen functional groups in GO paper played a major role in the electrical conductivity. Conductivity of GO paper was controlled by the presence of insulating sp^3 structure within the GO sheet. The functional groups break up the sp^2-hybridized structure of the stacked graphene sheets and generating electrically poor conducting behavior. GO_{110} displayed the ionic conductivity increased with increasing frequency about two orders compared to GO due to the removal of water molecules. This confirms that the increase in sp^2 cluster during the thermal reduction. A similar trend was observed for GO_{220} and was due to the elimination of oxygen functional groups. These results suggest the domination of conductive clusters and the removal of oxygen functional groups which are important for attaining maximum conductivity.

Fig. 10a indicates the behaviour of dielectric constant (ε') with respect to the applied frequency at 27 °C. The dielectric constant is a measure of charges stored inside the sample in the presence of applied electric field and detects the strength of alignment of dipoles in the dielectric. It is observed that the dielectric constant increases as frequency decreases due to interfacial polarization, which arises from space charges formed in the sample. In the presence of an electrical field, these space charges were confined by defects and localized accumulation of charge was formed at the electrode and sample interface. Therefore, ε' show the large values at low frequencies. Though the conductivity was high at higher frequencies, the electrons cannot follow the alternating electric field and so ε' of the GO paper was approximately constant and almost independent of frequency.

The behaviour of dielectric loss and imaginary parts of the complex dielectric modulus (M'') of GO was studied at 27 °C against the function of applied frequency (Fig. 10b). In general, dielectric loss (ε'') arising due to the loss of energy in a dielectric material through conduction (transport-related loss), slow polarization current (bipolar loss) and other deceptive phenomena like interfacial polarization contribution.[22,27,28] At low frequencies, dielectric loss showed the maximum value and was related to water intercalated into the GO. Increase of applied frequency decreases the loss and it approaches the stable value at high frequencies. Electric modulus was used to examine the dipole relaxation process, interfacial polarization and long-range conduction process within the bulk materials. The present study indicates the relaxation process associated with interfacial polarization clearly observed in the M'' curves of the GO.[29,30] Electrical modulus increases with increasing frequency and at certain frequency relaxation peak exist with a higher value. Here the, interfacial polarization appears only at certain frequencies for the GO and the electrical modulus drop to zero for higher frequencies.

GO_{110} showed the higher ε' with respect to applied frequency (Fig. 11a) than the GO and was attributed to interfacial polarization at low frequencies. The ε' and ε'' decreases with increasing frequency. Removal of adsorbed water molecules played a key role in the increased dielectric constant. The dielectric loss of GO_{110} was greatly improved due to increases of

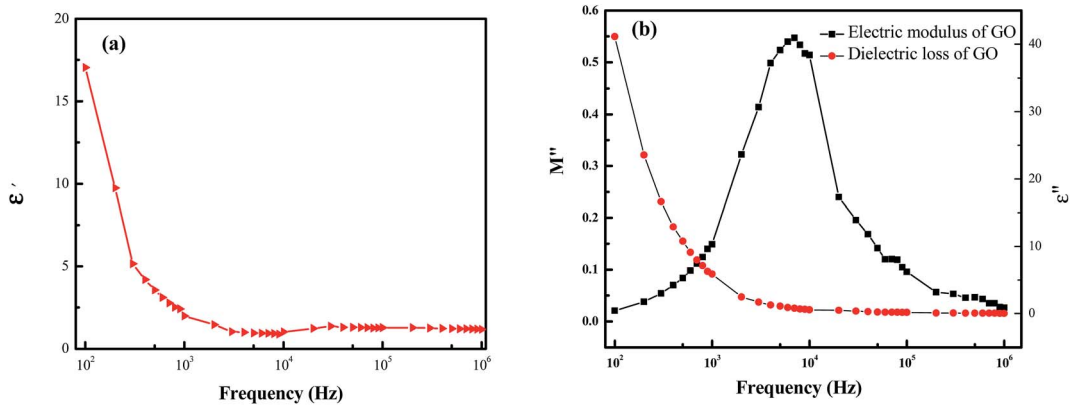

Fig. 10 (a) The variation of dielectric constant, (b) dielectric loss and imaginary part of the electric modulus with the applied frequency for pristine GO.

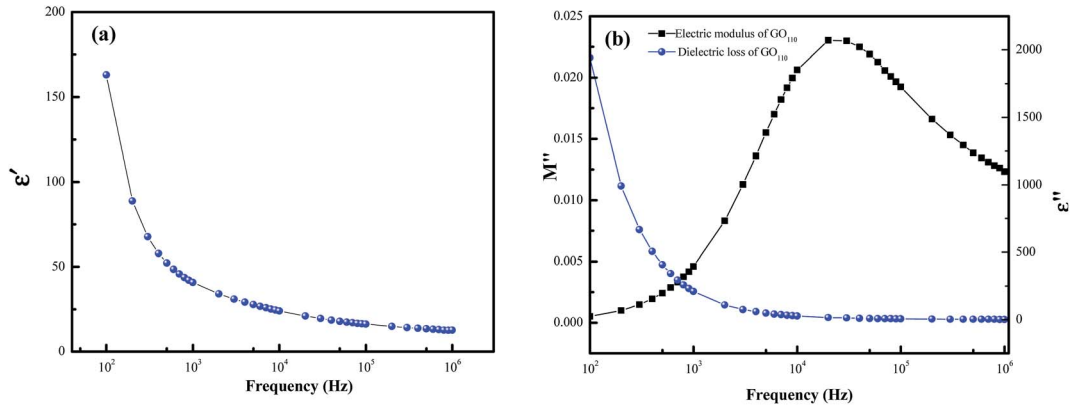

Fig. 11 (a) The variation of dielectric constant, (b) dielectric loss and imaginary part of the electric modulus with the applied frequency for 110 °C heat-treated GO.

conductive sp^2 clusters. Fig. 11b displays the imaginary part of the complex electrical modulus of GO_{110} with respect to applied frequency. Relaxation peak shifted towards the higher frequency compared to GO due to elimination of functional groups. Hence, the relaxation time decreases with the peak shifts towards the higher frequency region.

Meantime, GO_{220} showed the highest ε' and ε'' among the three samples (Fig. 12a and b). This property was arising from the domination of conductive sp^2 clusters after the restored sp^2 carbon atoms through the thermal reduction. Fig. 12b displays the imaginary part of the complex electrical modulus of GO_{220} against frequency. Relaxation peak was shifted towards the higher frequency region compared to GO, GO_{110} and was due to the elimination of functional groups in GO paper.

According to Huang *et al.* very high electrical conductivity, ε' and ε'' values have been measured in the order of 10^{-2} S m^{-1}, 10^5 and 10^9 respectively at 150 °C for GO. The present measurement on electrical conductivity of GO_{220}, was in the same order of earlier work. However, two and four orders lower ε' and ε'' than the literature was observed.[20] All the three samples have the strong frequency dependent of ε', ε'' and electrical modulus. The large value of ε' for GO_{220} was due to majority of conductive sp^2 clusters after the removal of insulating sp^3 through heat treatment. Moreover, ε'' occurs in GO_{220} was due to conduction, dipole and vibrational losses. The electrical conduction loss was due to elimination of functional groups, which in turn increases the dielectric loss.

In an optical fiber, when light crosses an interface between the core and modified cladding with different refractive indices, the light beam partially refracted and partially reflected at the interface depending on the angle of incidence. When the angle of incidence was equivalent to the critical angle, the light was reflected back into the core. The penetrated or refracted light intensity called evanescent field and its intensity decreasing exponentially away from the core–cladding interface. Evanescent waves in the cladding region was used for developing fiber optic gas sensors. Absorption of evanescent field phenomenon in the modified cladding region was studied through the variation of output light intensity to detect gas molecules. The total internal reflection was occurring at the interface between core and modified cladding when the refractive index of core was greater than the cladding of optical fiber.[23,24] Thus, a part of the light was penetrating into the cladding material, when the refractive index of modified cladding was higher than the core and enters the modified cladding–air interface. Variation of output light intensity occurs when the refractive indices of core

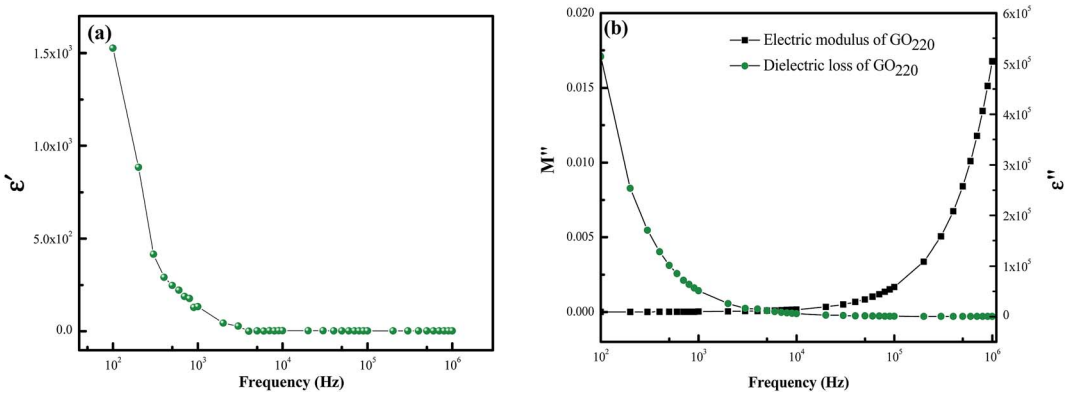

Fig. 12 (a) The variation of dielectric constant, (b) dielectric loss and imaginary part of the electric modulus with the applied frequency for 220 °C heat-treated GO.

(n_{core}) and modified cladding material (n_{mclad}) changes. When $n_{core} > n_{mclad}$, the total internal reflection occurs at core–cladding interface. The characteristics of gas sensing exhibits when $n_{core} < n_{mclad}$ and partial reflection of light occurs at the core–cladding interface and the light enters into the modified cladding. Loss of partially refracted light through the optical fiber leads to decrease in output intensity. The characteristic of gas sensing was occurred at the modified cladding–air interface. The total internal reflection occurred at this interface and re-entry of leaked light changed the output intensity.

Absorption of the evanescent field exists in the outer air medium. The light beam undergoes total internal reflection at the modified cladding–air interface and the intensity of output light would vary when the gas molecules interact with modified cladding. The loss of light intensity undergoes in the absence of the gas molecules because of evanescent wave absorption occur at the outer air medium. The evanescent wave absorption may be higher or lower than the reference value in the presence of gases and magnitude of evanescent wave absorption.[23] In the present study, as purchased PMMA raw fiber and cladding removed uncoated fiber were exposed to ammonia, ethanol and methanol vapors in the concentration range 0–500 ppm at 27 °C. No change in output intensity was observed in the absence of GO and heat-treated GO. The GO and heat-treated GO coated fibers were exposed to the water vapor to find out the interference of water vapor in the sensing performance. Interestingly, there is no remarkable response obtained during the exposure. The GO, GO_{110} and GO_{220} coated fibers were then tested in air atmosphere in the absence of test vapors. No change in output intensity was noticed and that output intensity was taken as reference intensity (reference or zero intensity mentioned by dotted line in Fig. 13) for sensing.

Variation of output light intensity was measured in the wavelength range 200 to 1000 nm during interaction between the test gases and the sensing material. Concentration of sensing gas was fixed in the range 0–500 ppm and varied in steps of 100 ppm. The maximum change in intensity was observed at a particular wavelength for each vapor and was taken for sensitivity calculation. In the case of pristine GO, GO_{110} and GO_{220} coated fibers exposed to NH_3 vapor, decrease (for GO and GO_{110}) and increase (GO_{220}) in output intensity (from the reference value) at 672 nm was observed as shown in ESI 1.† Similarly, the maximum wavelength responses for pristine GO, GO_{110} and GO_{220} coated fibers for ethanol/methanol vapors were observed as 675/672, 665/672 and 665/672 respectively and are shown in ESI 2–3.† These results indicate that the GO, GO_{110} and GO_{220} sheets were sensitive to the vapors.

Change in intensity from the reference value against vapor concentration of NH_3, ethanol and methanol for GO, GO_{110} and GO_{220} sensors were plotted in Fig. 13. Sensitivity of the fiber optic gas sensor was defined as the ratio of change in output intensity with that of change in concentration of test gas. Thus, the sensitivities of pristine GO, GO_{110} and GO_{220} coated sensors were found to be −33, −15 and +7 counts per 100 ppm respectively for NH_3 (Fig. 13a). In the case of ethanol vapor, sensitivities were calculated as −31, −15 and +6 counts per 100 ppm for GO, GO_{110} and GO_{220} respectively (Fig. 13b). Weak interaction between the polar groups in sensing material and the methanol vapor reflected on sensitivities and were calculated as −21, −9 and +3 counts per 100 ppm for GO, GO_{110} and GO_{220} respectively (Fig. 13c). Here the positive and negative signs are representing the increase and decrease in output intensities from the reference value of the fiber optic sensor. Interestingly, the pristine GO and GO_{110} coated fibers showed the decrease in output light intensity from the reference value against vapor concentration (ESI 1–2†). This was due to more evanescent field absorption at the boundary between GO/GO_{110} and test vapors. In contrast, GO_{220} coated sensor showed increased output light intensity from the reference value with respect to vapor concentration (ESI 3†). This was due to the less evanescent field absorption at the boundary between GO_{220} and the test vapors. Presence of oxygen functional groups in GO made the material hydrophilic. High surface area due to the exfoliation as observed in powder XRD provides the much better vapor sensing property than the heat-treated GO. Interaction between the oxygen functional groups in pristine GO and the test vapors were higher than the heat-treated samples due to the formation of intermolecular polar interactions.[31,32] Heat treatment lead to the removal of functional groups confirmed from

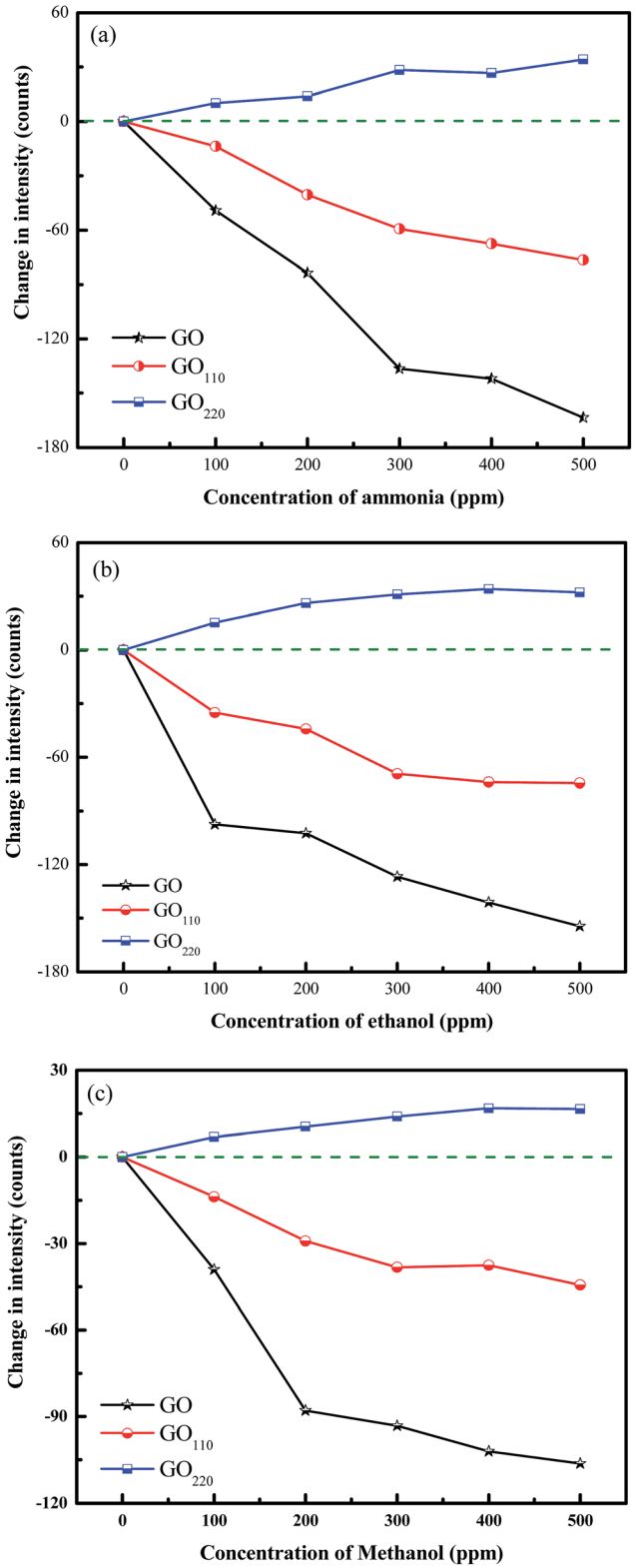

Fig. 13 Graph between a change in output intensity and gas concentration (0–500 ppm) of (a) ammonia (b) ethanol and (c) methanol for GO, GO_{110}, GO_{220}.

TGA and FT-IR made the materials became hydrophobic. The hydrophilic and hydrophobic nature of GO and heat-treated GO were further confirmed by dispersing the material in water. The GO dispersion in H_2O was stable even after three weeks and will be useful for water based solution processing. In contrast, sedimentation of GO_{110} and GO_{220} dispersed in H_2O was found after three hours, introduced limitations towards aqueous based processing.

In the present study, output light intensity variation arises predominantly due to physical adsorption of gas molecules on the surface of sensing materials. The refractive index of GO was controlled by the amount of hydroxyl and carboxyl functional groups through the interaction with analyte. In the case of NH_3 sensing, the –OH and –COO ions in GO were possibly involved in hydrogen bonding with ammonia. This results in changing the refractive index of the modified cladding and so decrease in output intensity. The pristine GO was hydrophilic and had more number of attached oxygen functional groups than the heat treated GO. Hence, the pristine GO showed better sensing performance than the heat treated GO. Thus, the evanescent wave absorption occurred at the modified cladding–air interface during the interaction of ammonia with GO. Here, the magnitude of absorption was higher than the pure air environment. In the low vapor concentration, ammonia molecules were adsorbed over the surface of the GO sheets till to reach the critical concentration. At the critical concentration and above, the coexistence of vapor and liquid phase of ammonia molecules did not interrupt much on the refractive index of modified cladding. At this juncture, thick layer of adsorbed ammonia was formed over GO sheets resulting minor change in output intensity. This hypothesis was confirmed through the attainment of saturation in output intensity after the critical concentration. Similar trend was observed for ethanol and methanol vapors with lesser sensitivities than the ammonia. Here, the hydrogen bondings between the –OH in alcohol and –OH/–COO ions in GO are responsible for sensing. Lesser electronegativity of alcohol than ammonia was reflected on the sensitivity variation. Thus, the experimental results clearly indicate the role of functional groups in fiber optic gas sensing.

Conclusion

GO was synthesized using modified Hummers method and reduced into GO_{110} and GO_{220} partially through thermal treatment under vacuum atmosphere. The existence of various oxygen functional groups in GO and heat-treated GO were characterized by powder X-ray diffraction, Fourier-transform infrared, micro Raman and UV-vis-NIR spectroscopy techniques. The sp^3 hybridized carbon atoms attached covalently with oxygen in the form of epoxy, carboxyl, hydroxyl and carbonyl groups suppressing the ionic conductivity of GO. GO_{220} had maximum conductivity in the order of 10^{-2} S m^{-1} obtained at 27 °C. Dielectric constant and loss of GO_{220} were calculated as 10^3 and 10^5 respectively. The GO, GO_{110} and GO_{220} coated fiber optic sensors were demonstrated for ammonia, ethanol and methanol vapors sensing at 27 °C. GO, GO_{110} and GO_{220} sensors provide a good prospect for use with low cost and comfort of device fabrication. High surface area, exfoliation of GO were observed using powder XRD offers better vapor sensing ability than the heat-treated GO. The sensitivities of GO sensor

were calculated as −0.32, −0.26 and −0.20 counts per ppm for ammonia, ethanol and methanol vapors respectively. The stable electrical and chemical properties of GO and heat treated GO have potential to produce flexible electronic devices, more sensitive fiber optic sensor and new photonic devices for room temperature applications.

Acknowledgements

We would like to thank Dr Justin Joseyphus, Mr T. Arun (NITT, India) for TGA characterization and Dr N. V. Giridharan, Mr M. Muneeswaran (NITT, India) for dielectric measurements.

References

1 S. Park and R. S. Ruoff, *Nat. Nanotechnol.*, 2009, **4**, 217–224.
2 D. A. Dikin, S. Stankovich, E. J. Zimney, R. D. Piner, G. H. B. Dommett, G. Evmenenko, S. T. Nguyen and R. S. Ruoff, *Nature*, 2007, **448**, 457–460.
3 Y. W. Zhu, S. Murali, W. W. Cai, X. S. Li, J. W. Suk, J. R. Potts and R. S. Ruoff, *Adv. Mater.*, 2010, **22**, 3906–3924.
4 K. S. Novoselov, A. K. Geim, S. V. Morozov, D. Jiang, Y. Zhang, S. V. Dubonos, I. V. Grigorieva and A. A. Firsov, *Science*, 2004, **306**, 666–669.
5 S. Stankovich, D. A. Dikin, R. D. Piner, K. A. Kohlhaas, A. Kleinhammes, Y. Jia, Y. Wu, S. B. T. Nguyen and R. S. Ruoff, *Carbon*, 2007, **45**, 1558–1565.
6 K. S. Kim, Y. Zhao, H. Jang, S. Y. Lee, J. M. Kim, K. S. Kim, J. H. Ahn, P. Kim, J. Y. Choi and B. H. Hong, *Nature*, 2009, **457**, 706–710.
7 X. Lu, M. Yu, H. Huang and R. S. Ruoff, *Nanotechnology*, 1999, **10**, 269–272.
8 G. Eda and M. Chhowalla, *Adv. Mater.*, 2010, **22**, 2392–2415.
9 G. Eda and M. Chhowalla, *Nano Lett.*, 2009, **9**, 814–818.
10 N. Mohanty and V. Berry, *Nano Lett.*, 2008, **8**, 4469–4476.
11 X. Wang, L. Zhi and K. Mullen, *Nano Lett.*, 2008, **8**, 323–327.
12 O. C. Compton and S. T. Nguyen, *Small*, 2010, **6**, 711–723.
13 S. Pei and H. M. Cheng, *Carbon*, 2012, **50**, 3210–3228.
14 H. J. Shin, K. K. Kim, A. Benayad, S. M. Yoon, H. K. Park, I. S. Jung, M. H. Jin, H. K. Jeong, J. M. Kim, J. Y. Choi and Y. H. Lee, *Adv. Funct. Mater.*, 2009, **199**, 1987–1992.
15 G. Wang, J. Yang, J. Park, X. Gou, B. Wang, H. Liu and J. Yao, *J. Phys. Chem. C*, 2008, **112**, 8192–8195.
16 J. Zhang, H. Yang, G. Shen, P. Cheng, J. Zhang and S. Guo, *Chem. Commun.*, 2010, **46**, 1112–1114.
17 F. Schedin, A. K. Geim, S. V. Morozov, E. W. Hill, P. Blake, M. I. Katsnelson and K. S. Novoselov, *Nat. Mater.*, 2007, **6**, 652–655.
18 J. T. Robinson, F. K. Perkins, E. S. Snow, Z. Wei and P. E. Sheehan, *Nano Lett.*, 2008, **8**, 3137–3140.
19 S. Some, Y. Xu, Y. Kim, Y. Yoon, H. Qin, A. Kulkarni, T. Kim and H. Lee, *Sci. Rep.*, 2013, **3**, 1868.
20 X. Huang, C. Zhi, P. Jiang, D. Golberg, Y. Bando and T. Tanaka, *Nanotechnology*, 2012, **23**, 455705.
21 W. S. Hummers and R. E. Offeman, *J. Am. Chem. Soc.*, 1958, **80**, 1339.
22 M. M. El-Nahass, H. A. M. Ali, M. Saadeldin and M. Zaghllol, *Phys. B*, 2012, **407**, 4453–4457.
23 B. Renganathan, D. Sastikumar, G. Gobi, N. R. Yogamalar and A. C. Bose, *Sens. Actuators, B*, 2011, **156**, 263–270.
24 S. Manivannan, A. M. Saranya, B. Renganathan, D. Sastikumar, G. Gobi and K. C. Park, *Sens. Actuators, B*, 2012, **171–172**, 634–638.
25 Z. Hu, Y. Chen, Q. Hou, R. Yin, F. Liua and H. Chena, *New J. Chem.*, 2012, **36**, 1373–1377.
26 S. Thakur and N. Karak, *Carbon*, 2012, **50**, 5331–5339.
27 M. M. El-Nahass and H. A. M. Ali, *Solid State Commun.*, 2012, **152**, 1084–1088.
28 J. Zhang, M. Mine, D. Zhu and M. Matsuo, *Carbon*, 2009, **47**, 1311–1320.
29 Y. Li, X. Huang, Z. Hu, P. Jiang, S. Li and T. Tanaka, *ACS Appl. Mater. Interfaces*, 2011, **3**, 4396–4403.
30 B. G. Soares, M. E. Leyva, G. M. O. Barra and D. Khastgir, *Eur. Polym. J.*, 2006, **42**, 676–686.
31 O. C. Compton, S. W. Cranford, K. W. Putz, Z. An, L. C. Brinson, M. J. Buehler and S. T. Nguyen, *ACS Nano*, 2012, **6**, 2008–2019.
32 J. I. Paredes, S. Villar-Rodil, A. Martinez-Alonso and J. M. D. Tascon, *Langmuir*, 2008, **24**, 10560–10564.